

Power limits and a figure of merit for stimulated Brillouin scattering in the presence of third and fifth order loss

C. Wolff,^{1,2*} P. Gutsche,^{2,3} M. J. Steel,^{1,4} B. J. Eggleton,^{1,5} and C. G. Poulton^{1,2}

¹ Centre for Ultrahigh bandwidth Devices for Optical Systems (CUDOS), Australia;

² School of Mathematical and Physical Sciences,
University of Technology Sydney, NSW 2007, Australia;

³ Zuse Institute Berlin, Takustraße 7, D14195 Berlin, Germany;

⁴ MQ Photonics Research Centre, Department of Physics and Astronomy,
Macquarie University Sydney, NSW 2109, Australia;

⁵ Institute of Photonics and Optical Science (IPOS), School of Physics,
University of Sydney, NSW 2006, Australia.

christian.wolff@uts.edu.au

Abstract: We derive a set of design guidelines and a figure of merit to aid the engineering process of on-chip waveguides for strong Stimulated Brillouin Scattering (SBS). To this end, we examine the impact of several types of loss on the total amplification of the Stokes wave that can be achieved via SBS. We account for linear loss and nonlinear loss of third order (two-photon absorption, 2PA) and fifth order, most notably 2PA-induced free carrier absorption (FCA). From this, we derive an upper bound for the output power of continuous-wave Brillouin-lasers and show that the optimal operating conditions and maximal realisable Stokes amplification of any given waveguide structure are determined by a dimensionless parameter \mathcal{F} involving the SBS-gain and all loss parameters. We provide simple expressions for optimal pump power, waveguide length and realisable amplification and demonstrate their utility in two example systems. Notably, we find that 2PA-induced FCA is a serious limitation to SBS in silicon and germanium for wavelengths shorter than 2200nm and 3600nm, respectively. In contrast, three-photon absorption is of no practical significance.

© 2024 Optical Society of America

OCIS codes: (); (); () .

References and links

1. R. W. Boyd, *Nonlinear optics* (Academic, 3rd ed., 2003).
2. L. Brillouin. "Diffusion de la lumière par un corps transparent homogène," *Annals of Physics* **17**, 88–122 (1922).
3. R. Y. Chiao, C. H. Townes, and B. P. Stoicheff, "Stimulated Brillouin scattering and coherent generation of intense hypersonic waves," *Phys. Rev. Lett.* **12**, 592 (1964).
4. G. P. Agrawal, *Nonlinear fiber optics* (Academic, 5th ed., 2012).
5. M. S. Kang, A. Nazarkin, A. Brenn, and P. St. J. Russell, "Tightly trapped acoustic phonons in photonic crystal fibres as highly nonlinear artificial Ramanoscillators, " *Nature Phys.* **5**, 276–280 (2009).
6. R. Pant, C. G. Poulton, D.-Y. Choi, H. Mcfarlane, S. Hile, E. Li, L. Thévenaz, B. Luther-Davies, S. J. Madden, and B. J. Eggleton, "On-chip stimulated Brillouin scattering," *Opt. Express* **19**, 8285–8290 (2011).

7. W. Qiu, P. T. Rakich, H. Shin, H. Dong, M. Soljačić, and Z. Wang, “Stimulated Brillouin scattering in nanoscale silicon step-index waveguides: a general framework of selection rules and calculating SBS gain,” *Opt. Express* **21**, 31402–31419 (2013).
8. H. Shin, W. Qiu, R. Jarecki, J. A. Cox, R. H. Olsson III, A. Starbuck, Z. Wang, and P. T. Rakich, “Tailorable stimulated Brillouin scattering in nanoscale silicon waveguides,” *Nat. Commun.* **4**, 1944 (2013).
9. R. Van Laer, B. Kuyken, D. Van Thourhout, and R. Baets, “Interaction between light and highly confined hypersound in a silicon photonic nanowire,” *Nature Photon.* **9**, 199 (2015).
10. I. V. Kabakova, R. Pant, D.-Y. Choi, S. Debbarma, B. Luther-Davies, S. J. Madden, and B. J. Eggleton, “Narrow linewidth Brillouin laser based on chalcogenide photonic chip,” *Opt. Lett.* **38**, 3208–3211 (2013).
11. T. F. S. Buettner, I. V. Kabakova, D. D. Hudson, R. Pant, C. G. Poulton, A. Judge, and B. J. Eggleton, “Phase-locking in Multi-Frequency Brillouin Oscillator via Four Wave Mixing,” *Sci. Rep.* **4**, 5032 (2014).
12. X. Huang and S. Fan, “Complete all-optical silica fiber isolator via Stimulated Brillouin Scattering,” *J. Lightwave Technol.* **29**, 2267–2275 (2011).
13. I. Aryanfar, C. Wolff, M. J. Steel, B. J. Eggleton, and C. G. Poulton, “Mode conversion using stimulated Brillouin scattering in nanophotonic silicon waveguides,” *Opt. Express* **22**, 29270–29282 (2014).
14. L. Thévenaz, “Slow and fast light in optical fibres,” *Nature Photon.* **2**, 474–481 (2008).
15. B. Vidal, M. A. Piqueras, and J. Marti, “Tunable and reconfigurable photonic microwave filter based on stimulated Brillouin scattering,” *Opt. Lett.* **32**, 23–25 (2007).
16. J. Li, H. Lee, and K. J. Vahala, “Microwave synthesizer using an on-chip Brillouin oscillator,” *Nat. Commun.* **4**, 2097 (2013).
17. B. Morrison, D. Marpaung, R. Pant, E. Li, D.-Y. Choi, S. Madden, B. Luther-Davies, and B. J. Eggleton, “Tunable microwave photonic notch filter using on-chip stimulated Brillouin scattering,” *Opt. Commun.* **313**, 85–89 (2014).
18. C. Wolff, P. Gutsche, M. J. Steel, B. J. Eggleton, and C. G. Poulton, “Impact of nonlinear loss on Stimulated Brillouin Scattering,” *J. Opt. Soc. Am. B* (accepted) *arXiv:1505.02517 [physics.optics]*.
19. I. D. Rukhlenko, M. Premaratne, G. P. Agrawal, “Nonlinear Silicon Photonics: Analytical Tools,” *IEEE J. Sel. Top. Quantum Electron.* **16**, 200–215 (2010).
20. C. Wolff, M. J. Steel, B. J. Eggleton, and C. G. Poulton, “Stimulated Brillouin Scattering in integrated photonic waveguides: forces, scattering mechanisms and coupled mode analysis,” *Phys. Rev. A* **92**, 013836 (2015).
21. B.G. Helme, P.J. King, “The Phonon Viscosity Tensor of Si, Ge, GaAs, and InSb,” *phys. stat. sol. (a)* **45**, K33 (1978).
22. R. Van Laer, B. Kuyken, R. Baets, D. Van Thourhout “Unifying Brillouin scattering and cavity optomechanics,” *arXiv:1503.03044 [physics.optics]*, (2015).
23. J.J. Wortman, R.A. Evans “Young’s Modulus, Shear Modulus, and Poisson’s Ratio in Silicon and Germanium,” *J. Appl. Phys.* **36**, 153 (1965).
24. D.K. Biegelsen, “Photoelastic Tensor of Silicon and the Volume Dependence of the Average Gap,” *Phys. Rev. Lett.* **32**, 1196 (1974).
25. A. Feldman, R.M. Waxler, D. Horowitz, “Photoelastic constants of germanium,” *J. Appl. Phys.* **49**, 2589 (1978).
26. A. D. Bristow, N. Rotenberg and H. M. Van Driel “Two-photon absorption and Kerr coefficients of silicon for 850–2200 nm,” *Appl. Phys. Lett.* **90**, 191104 (2007).
27. D. Seo, J. M. Gregory, L. C. Feldman, N. H. Tolk, and P. I. Cohen, “Multiphoton absorption in germanium using pulsed infrared free-electron laser radiation,” *Phys. Rev. B* **83**, 195203 (2011).
28. S. Pearl, N. Rotenberg, and H. M. van Driel, “Three photon absorption in silicon for 2300–3300 nm,” *Appl. Phys. Lett.* **93**, 131102 (2008).

1. Introduction

Stimulated Brillouin Scattering (SBS) is the coherent and self-amplifying interaction between light waves and a hypersonic acoustic wave that are confined in the same waveguide or bulk material [1]. Initially predicted by Brillouin [2] and first observed in quartz [3], it has been well known for many years in optical fibers as a highly resonant and strong third-order nonlinearity in both backward [4] and forward directions [5]. More recently, there has been an intense research effort to generate SBS in on-chip waveguides: SBS has been observed in chalcogenide glass rib waveguides [6] and, inspired by theoretical considerations [7], silicon nanowires [8, 9]. These experiments have greatly broadened the applicability of SBS to include a large number of on-chip applications, such as powerful narrow-band light sources [10, 11], non-reciprocal light propagation [12, 13], slow light [14] and signal processing in the context of microwave photonics [15–17].

The realisation of SBS in any device hinges on achieving sufficient Stokes amplification

within the device length to be useful. Within the basic theory, where SBS is the only nonlinear process present, the amplification of the Stokes wave (i.e. the ratio of Stokes power at the output to injected Stokes power) is proportional to the power of the injected pump beam; the Stokes wave initially exhibits exponential growth until it starts to deplete the pump. In reality, however, neither this exponential growth, nor the predicted linear relationship between amplification and pump power, can be expected over the whole range of pump powers. The reason for this is nonlinear loss in the waveguide, where third-order processes – particularly two-photon absorption (2PA) – impact the SBS-performance quite differently from fifth-order processes such as three-photon absorption (3PA) and 2PA-induced free carrier absorption (FCA). The latter is a major nonlinear loss mechanism in group-IV semiconductors such as silicon and germanium in important wavelength ranges. These materials are of interest because many promising applications of SBS require the integration of SBS-gain in group-IV photonic circuits in order to benefit from CMOS-type fabrication techniques for mass production and integration with electronic circuitry.

In this paper, we apply recent analytic work [18] to examine the limitations that nonlinear loss imposes on the gain for SBS. The related effect of nonlinear loss in Stimulated Raman Scattering has been investigated [19] although based on different approximations and with an emphasis on short-pulse propagation and pump depletion. In contrast, we present two important findings: firstly, that there is an upper bound for the output Stokes *power* that can be obtained with a specific waveguide design (i.e. for a specific geometry of the waveguide cross-section with a specific choice of materials) by amplifying a weak (e.g. thermal) initial Stokes signal. This bound, which involves both nonlinear loss coefficients and the SBS-gain parameter of the design, in particular represents an absolute upper bound for the output power of any continuous wave (CW) Brillouin-laser. Secondly, we find that the total *amplification* (ratio of output to input power) of an incident Stokes wave that can be obtained with a specific waveguide design also has an upper bound. This maximally realisable amplification and the corresponding optimal operating conditions are determined by a dimensionless *figure of merit*, which involves only the effective coefficients for the linear waveguide loss, the 2PA, the 2PA-induced FCA and the SBS-gain coefficient. Our figure of merit forms a valuable engineering tool for the design of SBS-active waveguides since it provides a convenient way to compare the performance of different designs and yields good estimates for the waveguide length and pump power. We demonstrate this in the last section of the paper using two types of suspended silicon nanowires in backward SBS configuration as examples.

2. Approach

We choose to describe the problem within our coupled-mode framework [20] for SBS in an integrated waveguide, which is assumed to extend in the positive z -direction. When focusing on strongly confining waveguides, as in this paper, it is appropriate to express the optical fields in terms of power carried by the individual waveguide modes, although other formulations are possible, e.g. based on field intensities as is common in bulk nonlinear optics. The equations of motion for the power $P^{(1)}(z)$ carried in the Stokes wave and the power $P^{(2)}(z)$ in the pump wave are

$$s\partial_z P^{(1)} = (\Gamma - 2\beta - \gamma P^{(2)})P^{(2)}P^{(1)} - \alpha P^{(1)} + C_1, \quad (1)$$

$$\partial_z P^{(2)} = -(\beta + \gamma P^{(2)})[P^{(2)}]^2 - \alpha P^{(2)} + C_2, \quad (2)$$

where the symbol s is used to describe both forward SBS ($s = +1$) and backward SBS ($s = -1$) within a common framework. Here $\Gamma = \int dr^2 \mathbf{u}^* \cdot \mathbf{f}$ is the overlap integral between the optical force distribution (involving both electrostriction and radiation pressure) as known from the

literature [7, 20]. The acoustic angular frequency Ω is defined by the acoustic dispersion relation and the optical wave number via the usual phase matching condition [7, 20]. Later we will also provide theoretical estimates for the Brillouin line width $\Delta\Omega$, which we compute from the overlap integral [20] between the acoustic eigenmodes and the dynamic viscosity of silicon and germanium [21].

The linear loss coefficient α , 2PA-coefficient β , and coefficient γ for 2PA-induced FCA are overlap integrals of the optical eigenmodes and the respective dissipative nonlinear polarization currents as presented e.g. in Ref. [18].

The two large-signal correction terms

$$C_1 = -(\beta + \gamma P^{(1)} + 4\gamma P^{(2)})[P^{(1)}]^2, \quad (3)$$

$$C_2 = -(2\beta + \Gamma + 4\gamma P^{(2)} + \gamma P^{(1)})P^{(1)}P^{(2)} \quad (4)$$

can be neglected when assuming that the Stokes wave is weak compared to the pump wave, which we refer to as the small-signal approximation. Within this approximation, forward and backward SBS yield the same results for the power and amplification limits. We have assumed quasi-CW light and have absorbed the acoustic envelope into Γ via a local acoustic response approximation. This is justified if the optical modes vary on a length scale large compared to the acoustic decay length [20]; in particular, the optical loss must be sufficiently low [22].

Equations (1–4) are derived in detail in Ref. [18] and we restrict ourselves here to a brief description of the nonlinear loss terms. The terms involving β describe 2PA due to power carried in the respective mode itself (prefactor β) and due to the combination of both modes (prefactor 2β). The nontrivial factor 2 arises because interference between the modes leads to a non-uniform intensity distribution; it appears commonly in nonlinear optics [19]. The terms involving γ describe fifth-order loss (mainly 2PA-induced FCA) and as before appear as loss induced by either mode alone (prefactor γ) and cross terms that describe the contribution of inter-mode interference to the 2PA-induced FCA (prefactor 4γ). The nontrivial factor 4 arises in a similar fashion [18] as in the case of 2PA, but is less commonly encountered.

For waveguides with eigenmodes that differ strongly from plane waves (e.g. silicon nanowires), the coefficients Γ, α, β and γ depend sensitively on the geometry and eigenmode field distributions in the transversal plane. In the case of waveguides with plane wave-like eigenmodes (e.g. silica fibers), the optical powers can be replaced with local intensities and the parameters with established parameters [1, 4]. This is equivalent to normalising the eigenmode (i.e. plane wave) over a cross section of 1 m^2 within our framework.

Finally, we note that inter-mode SBS can be described by the same equations at the expense of a more convoluted notation, leading to analogous results with modified parameters (see appendix).

3. Maximal output power

We begin with the output power upper bound. From the large-signal Stokes equation [i.e. Eqs. (1,3)] we find

$$s\partial_z P^{(1)} < [\Gamma - 2\beta - 4\gamma P^{(1)} - \gamma P^{(2)}]P^{(1)}P^{(2)}. \quad (5)$$

In conjunction with the requirement $s\partial_z P^{(1)} > 0$ expressing Stokes amplification, this provides a necessary (though not tight) upper bound for the output power:

$$P^{(1)} < \frac{\Gamma - 2\beta - 4\gamma P^{(2)}}{4\gamma} < \frac{\mathcal{P}}{4}, \quad (6)$$

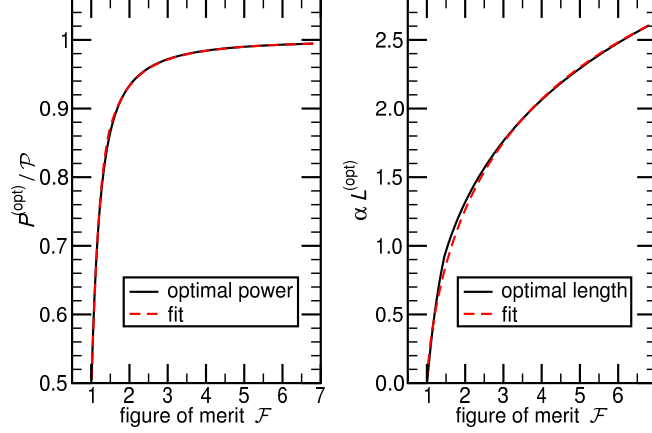


Fig. 1. Optimal pump power (left panel) and optimal waveguide length (right panel) as functions of the figure of merit \mathcal{F} [see Eq. (12)]; numerical results (black solid lines) in comparison to the approximate expressions Eq. (14) and Eq. (13) (red dashed lines). The optimal pump power is between $\mathcal{P}/2$ and \mathcal{P} and the optimal waveguide length is of order α^{-1} .

where we have introduced the natural unit of power

$$\mathcal{P} = (\Gamma - 2\beta)/\gamma. \quad (7)$$

Any greater Stokes power level will necessarily decay with propagation and the maximum power limit can only be exceeded anywhere in the waveguide if it is exceeded at the input face. Notably, Eq. (6) is an absolute upper bound for the output power of any CW Brillouin-laser. This should be distinguished from the influence of linear loss, which mainly influences the laser threshold and the line width. Note also that the simple expression $\mathcal{P}/4$ overestimates the maximal output power because of the term $4\gamma P^{(2)}$ and further nonlinear loss terms, which were removed in arriving at the inequality Eq. (5).

4. Maximal amplification and optimal design parameters

The discussion of optimal design parameters and figures of merit is based on the small-signal equations, i.e. Eqs. (1,2) under the approximation $C_1 = C_2 = 0$. As a result, we obtain upper bounds for both the pump wave and the Stokes wave power levels, and, therefore, for the measurable total Stokes amplification of a given waveguide. This can be concluded from the fact that the neglected terms Eqs. (3,4) are strictly negative. The small-signal equations can be solved analytically for the case $\beta = 0$ and starting from this solution, the case of $\beta \neq 0$ can be treated perturbatively [18]. In order to strip the problem of as many free parameters as possible, it is advisable to express all powers with respect to the natural power unit \mathcal{P} introduced in Eq. (7) and to express all lengths with respect to the corresponding natural length unit

$$\Lambda = \gamma/(\Gamma - 2\beta)^2. \quad (8)$$

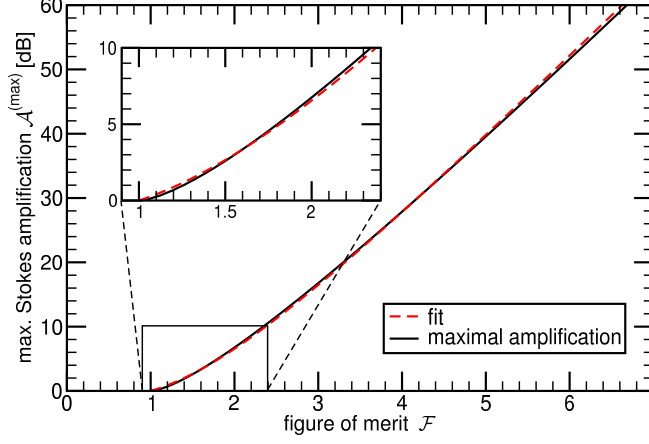


Fig. 2. The maximally realisable Stokes amplification for FCA-dominated setups as a function of the figure of merit \mathcal{F} [see Eq. (12)] computed numerically (black solid line) and approximate fit according to Eq. (15) (red dashed line). Materials and waveguide designs with $\mathcal{F} < 1$ cannot amplify an injected Stokes wave.

We thus obtain an analytical expression that predicts the total Stokes amplification \mathcal{A} as a function of the waveguide length L and the injected pump power $P^{(2)}(0) = P_0$:

$$\mathcal{A}(L, P_0) = 10 \log_{10} \left[\frac{P^{(1)}(L)}{P^{(1)}(0)} \right] \text{ dB} \quad (9)$$

$$= \frac{10}{\ln 10} \left\{ \frac{1}{\sqrt{\alpha\Lambda}} \left[\tan^{-1} \sqrt{(1+\psi)\exp(2\alpha L) - 1} - \tan^{-1} \psi \right] - \frac{1}{2} \ln \left[\frac{(1+\psi)\exp(2\alpha L) - 1}{\psi} \right] \right\} \text{ dB}, \quad (10)$$

where $\psi = \alpha/(\gamma P_0^2)$ is a measure of the relative strength of linear loss and 2PA-induced FCA. The factor $1/\sqrt{\alpha\Lambda} = (\Gamma - 2\beta)/\sqrt{\alpha\gamma}$ in front of the first term of Eq. (10) is of particular interest, because it arises naturally from Eq. (1) by requiring that a positive $P^{(2)}$ exists such that $s\partial_z P^{(1)} > 0$ (i.e. Stokes amplification at some positive pump power). Since all coefficients are positive, this is only possible if

$$P^{(2)} = \frac{1}{2\gamma} \left[(\Gamma - 2\beta) \pm \sqrt{(2\beta - \Gamma)^2 - 4\alpha\gamma} \right] > 0; \quad \Rightarrow \quad \frac{\Gamma - 2\beta}{2\sqrt{\alpha\gamma}} > 1. \quad (11)$$

This is a necessary condition for any amplification of the Stokes wave. Therefore the quantity

$$\mathcal{F} = \frac{\Gamma - 2\beta}{2\sqrt{\alpha\gamma}} \quad (12)$$

lends itself as a *figure of merit* for SBS in waveguide designs.

Every \mathcal{F} corresponds to a different maximally realisable Stokes amplification $\mathcal{A}^{(\max)}$ and, through (10), this amplification is only obtained for a specific (optimal) choice of waveguide length $L^{(\text{opt})}$ and pump power $P^{(\text{opt})}$. We determined these values by numerically finding the maximum of $\mathcal{A}(L, P_0)$ for a wide range of \mathcal{F} and show them as black solid lines in Fig. 1 and Fig. 2. Observe that the worse the figure of merit, the weaker the pump and shorter the waveguide that delivers the optimal performance: since FCA is a fifth-order process while the SBS

Table 1. Table of nonlinear coefficients (Γ , β , γ), acoustic frequency $\Omega/2\pi$, Brillouin line width $\Delta\Omega/2\pi$, SBS-figure of merit \mathcal{F} , maximally realisable Stokes amplification $\mathcal{A}^{(max)}$ and the natural unit of power \mathcal{P} (four times the max. SBS-laser output power in case of $\mathcal{F} > 1$) for *bulk* silicon and germanium at wavelengths on the red and the blue side of the 2PA-threshold. We assumed a linear loss of $\alpha = 0.1$ dB/cm and a carrier life time of 10 ns throughout. The quantities Γ and Ω were computed from literature expressions [20] assuming wave propagation along the [100]-direction and purely electrostrictive coupling based on literature photoelastic coefficients [24, 25]. The Brillouin line width was computed as described in the main text using literature values for the dynamic viscosity [21]. The bulk 2PA-, 3PA- and FCA-coefficients are literature values [26–28] (annotated in the square brackets). As mentioned in the main text, this table lists bulk parameters, which are naturally expressed as power *intensities* (units of W/m²) rather than powers; this is reflected in the units for \mathcal{A} , β , γ and \mathcal{P} and $P^{(opt)}$, which differ from those in Table 2. Note that the photo-elastic tensor and the dynamic viscosity are available in the literature only for selected wavelengths, so we assumed them to be nondispersive, leading to a wavelength-independent prediction of the SBS-gain.

| | Silicon | | | Germanium | | | Unit |
|-----------------------|----------------------|----------------------|---------------------------|---------------------|---------------------|---------------------------|-----------------------|
| λ_0 | 1550 | 2000 | 2400 | 3000 | 3600 | 4000 | nm |
| $\Omega/2\pi$ | 38.1 | 29.5 | 24.6 | 13.2 | 11.0 | 9.90 | GHz |
| $\Delta\Omega/2\pi$ | 162 | 97 | 30 | 39 | 27 | 22 | MHz |
| Γ | 2.55 | 2.55 | 2.55 | 324 | 324 | 324 | mm/GW |
| α | 2.3 | 2.3 | 2.3 | 2.3 | 2.3 | 2.3 | m ⁻¹ |
| β | 15 ^[26] | 3 ^[26] | 0* | 200 ^[27] | 0.9 ^[27] | 0* | mm/GW |
| γ^\dagger | 0.29 ^[26] | 0.08 ^[26] | 3.5×10^{-5} [28] | 240 ^[27] | 1.1 ^[27] | 2.7×10^{-4} [27] | mm/(GW ²) |
| \mathcal{P} | – | – | 7200 | – | 0.29 | 1200 | W/(μm^2) |
| \mathcal{F} | –0.54 | –0.13 | 4.5 | –0.06 | 3.2 | 410 | – |
| $L^{(opt)}$ | – | – | 0.95 | – | 0.79 | 2.6 | m |
| $P^{(opt)}$ | – | – | 7100 | – | 0.28 | 1200 | W/(μm^2) |
| $\mathcal{A}^{(max)}$ | – | – | 34 | – | 19 | $\gg 60^\ddagger$ | dB |

* three photon absorption is the leading multiphoton process at this wavelength

† assuming 10 ns carrier life time

‡ only a very rough lower bound since our fit [Eq. (15)] only covers the range $\mathcal{F} < 7$

gain and 2PA are third-order processes, trying to drive a poor system harder is counterproductive.

The numerically obtained relationships between \mathcal{F} (in the range $\mathcal{F} > 1$) and the performance and operation parameters can be represented by three phenomenological fit functions

$$L^{(opt)} \approx (2 \ln \mathcal{F})^{0.713} \alpha^{-1}, \quad (13)$$

$$P^{(opt)} \approx \left(1 - 0.25 \mathcal{F}^{-2} - 0.25 \mathcal{F}^{-6}\right) \mathcal{P}, \quad (14)$$

$$\mathcal{A}^{(max)} \approx 13.0 \left[\sqrt{\mathcal{F}(\mathcal{F} - 1) + 3.0} - \sqrt{3.0} \right] \text{ dB}. \quad (15)$$

These expressions are provided as a convenient way to predict the maximal amplification and optimal waveguide length and pump power in the process of designing an SBS-active waveguide. Their good accuracy over a wide parameter range is demonstrated by Fig. 1 and Fig. 2, where they are shown as red dashed curves.

As mentioned, the interpretation of Eq. (12) as a figure of merit is based on the fact that a material or waveguide design with $\mathcal{F} < 1$ cannot amplify a Stokes wave. For $\mathcal{F} > 1$, Stokes

Table 2. Table of SBS-resonance parameters, loss parameters, SBS-figure of merit, maximally realisable Stokes-amplification and optimal operating conditions for two simple suspended nanowire designs (see Fig. 3) operated in backward SBS configuration in the 2PA-regime. The effective waveguide coefficients were computed in analogy to and using material parameters listed in Table 1, yet using the specified optical and best-suited acoustic eigenmodes. The SBS-gain coefficient includes both electrostriction and radiation pressure terms as described in the literature [20]. Furthermore, we show data for an experimentally studied geometry [9], where we adopted the SBS-parameters (gain, shift, linewidth), the linear loss and the carrier life time published for that particular structure and computed the nonlinear loss and from this \mathcal{F} , \mathcal{P} and and extrapolated $\mathcal{A}^{(\max)}$. Optimal operation conditions cannot be provided, because this structure does not provide net Stokes amplification.

| | E_x -wire BSBS | | | E_y -wire BSBS | | | Ref. [9] FSBS | Unit |
|------------------------|---------------------|-------|-------|---------------------|------|------|-------------------|------------------------------|
| λ_0 | 1550 | 2000 | 2000 | 1550 | 2000 | 2000 | 1550 | nm |
| width | 315* | 406* | 406* | 372* | 480* | 480* | 450 [†] | nm |
| height | 284* | 365* | 365* | 256* | 330* | 330* | 230 [†] | nm |
| $\Omega/2\pi$ | 12.3 | 9.56 | 9.56 | 10.2 | 7.92 | 7.92 | 9.2 [‡] | GHz |
| $\Delta\Omega/2\pi$ | 8.37 | 5.03 | 5.03 | 4.79 | 2.88 | 2.88 | 30 [‡] | MHz |
| Γ | 1210 | 729 | 729 | 4910 | 2950 | 2950 | 3218 [‡] | $\text{W}^{-1}\text{m}^{-1}$ |
| α | 23 | 23 | 4.6 | 23 | 23 | 4.6 | 60 [‡] | m^{-1} |
| β | 380 | 46 | 46 | 290 | 36 | 36 | 84 | $\text{W}^{-1}\text{m}^{-1}$ |
| γ^\dagger | 138000 | 13000 | 13000 | 105000 | 9900 | 9900 | 43800 | $\text{W}^{-2}\text{m}^{-1}$ |
| τ_c | 10 | 10 | 10 | 10 | 10 | 10 | 6 [‡] | ns |
| \mathcal{P} | 3 | 49 | 49 | 41 | 290 | 290 | 18 | mW |
| \mathcal{F} | 0.13 | 0.58 | 1.30 | 1.52 | 1.68 | 5.31 | 0.94 | – |
| $L^{(\text{opt})}$ | – | – | 137 | 38 | 45 | 514 | – | mm |
| $P^{(\text{opt})}$ | – | – | 39 | 36 | 261 | 287 | – | mW |
| $\mathcal{A}^{(\max)}$ | < 0 | < 0 | 1.4 | 2.8 | 3.9 | 44 | –0.2 [◊] | dB |

* geometry is scaled with the operating wavelength

[†] computed assuming the carrier life τ_c

[‡] value taken from Ref. [9]

[◊] extrapolated using Eq. (15) slightly outside its intended parameter range

amplification is possible, but the realisable amplification factor is limited to a number given by Eq. (15). For values $0 < \mathcal{F} < 1$, SBS generation of the Stokes wave occurs in pump-probe experiments with externally injected Stokes seeds, but with net attenuation along the waveguide. However, the regime of $\mathcal{F} > 1$ can still be reached by reducing the linear or fifth-order loss terms e.g. via free carrier extraction techniques. Finally, for $\mathcal{F} < 0$, SBS is overcome by the competing two-photon absorption irrespective of pump power (since both SBS and 2PA are third-order processes) or waveguide length, and no SBS-allowed regime can be reached by adjusting α or γ .

5. Examples and Conclusions

We demonstrate the utility of our figure of merit by discussing bulk silicon, bulk germanium, and three (two theoretical, one experimentally realised) silicon nanowire systems. In the case of bulk materials, the previously presented theory applies directly on replacing powers with power densities and effective waveguide loss and gain coefficients with the respective bulk material parameters. This is presented in Table 1 for the case of silicon and germanium at wavelengths

around the 2PA-threshold. Since this table contains numbers for SBS in bulk, only backward-SBS is possible and the SBS-gain is entirely defined by electrostriction and photoelasticity; radiation pressure does not contribute in Table 1. The SBS-gain and acoustic parameters were computed according to established methods for waveguides [7, 20] using periodic boundary conditions in the transverse plane and literature values for the mechanical and photoelastic parameters [23–25]. The acoustic line width $\Delta\Omega$ was computed from the acoustic group velocity and the acoustic decay parameter α_{ph} , which in turn was computed from the dynamic viscosity [20, 21]. The nonlinear loss parameters are literature values [26–28]. It is clearly visible that bulk silicon and germanium are ill-suited for SBS on the blue side (shorter wavelengths, higher frequencies) of their respective 2PA-thresholds ($\approx 2300\text{ nm}$ and $\approx 3650\text{ nm}$, respectively). This is mainly due to the combination of insufficient photoelastic coupling, high acoustic frequency (entailing high mechanical loss) and the strong fifth-order absorption term caused by 2PA-induced free carriers. However, we find that the fifth-order loss caused by 3PA allows for substantial figures of merit and should be negligible in practice. Therefore, SBS in bulk and quasi-bulk silicon and germanium seems infeasible in the near-IR and should be studied in the mid-IR.

Furthermore, we present numerical calculations of figures of merit for two theoretical nanowire designs at two different wavelengths and one experimental silicon nanowire at 1550 nm . The two theoretical structures together with the relevant optical modes are depicted in Fig. 3; note that the second example is not operated with the fundamental optical mode. For both waveguides, we computed the backward-SBS coupling (involving both electrostriction and radiation pressure) with the lowest few acoustic modes and present the results for the lowest quasi-longitudinal mode. Again, we computed the SBS-parameters and effective nonlinear coefficients using established methods [7, 18, 20] and literature material parameters [21, 23, 24, 26]. The results are shown in Table 2. For the theoretical structures, we have to choose a value for the linear loss, a quantity which is still improving with fabrication developments. We present results for 1 dB/cm (as a typical current value) for calculations at both wavelengths (columns 2,3,5,6), and for 0.2 dB/cm as a state of the art value for the calculations at $\lambda_0 = 2000\text{ nm}$ only (columns 4,7).

The results indicate that both designs can support SBS (i.e. $\mathcal{F} > 0$) at both considered wavelengths. However, neither of them is expected to provide net Stokes amplification on the blue side of the 2PA-threshold unless the linear loss is reduced considerably below 1 dB/cm . We find it noteworthy that our proposal for a waveguide based on the E_y -polarized eigenmode is predicted to provide higher SBS-gain than the previously studied E_x -polarized eigenmode.

For the comparison with the experimental structure, we adopted the geometry, published forward SBS-parameters and linear loss of a nearly suspended silicon nanowire [9] and complemented this with our numerically computed nonlinear loss coefficients based on the carrier life time measured in that structure. The first observation is that we find a figure of merit just below 1 corresponding to an extrapolated total Stokes amplification of -0.2 dB in agreement with the published value of -0.1 dB . As the natural power unit we find $\mathcal{P} = 18\text{ mW}$, which is 1.5 dB less than the published 2PA-threshold of 25 mW ; however, care should be taken when comparing the results, since the experimental 2PA-threshold gain was determined from Fig. 3a in Ref. [9], which depicts an on/off-gain, while we derived \mathcal{P} in the context of optimal net Stokes amplification.

In their paper, the authors of the experimental study mention that their device is close to net amplification. In fact, a reduction of the linear loss from the reported 2.6 dB/cm to 1 dB/cm would lead to a $\mathcal{F} = 1.5$, which would allow for a maximum net Stokes amplification of 2.7 dB realised for a waveguide of 37 mm and a pump power of 16 mW . In contrast, a reduction of the carrier life time to 2 ns would lead to a similar $\mathcal{F} = 1.6$, but the maximum Stokes amplification

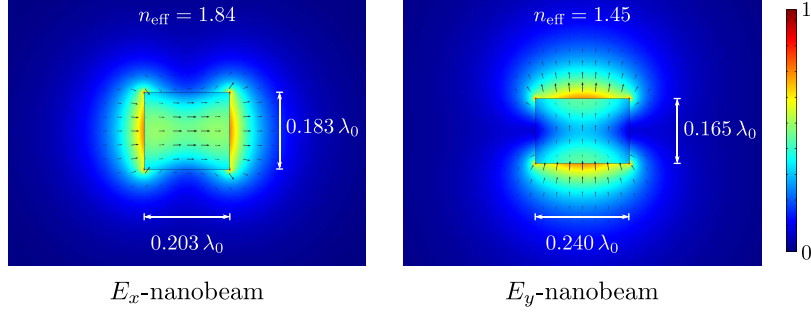


Fig. 3. Waveguide geometries and effective indices of the optical modes that are studied for backward SBS in Table 2. The color-plot depicts the modulus of the modal electric field in arbitrary units, the black arrows indicate the in-plane electric field components. The waveguides consist of silicon in [100]-orientation; their cross-sections are shown as a thin black rectangle and are scaled with the light's vacuum wavelength λ_0 .

of 3.4 dB would be achieved for a length of only 16 mm and a considerably higher pump power of 48 mW. The output powers of hypothetical CW SBS-laser using those two improved structures would be limited to less than 9 mW and 27 mW, respectively. This example illustrates how the results and parameter fits presented in this paper can help in designing the optimal length of samples and hint at the best route to improve performance.

In summary, we have studied the impact of third-order and fifth-order loss on the process of SBS in semiconductor waveguides. First, we derived an upper bound to the output power of an SBS-based amplifier. Second, we introduced a figure of merit as a simple measure of the suitability of an SBS-design and provide simple fit functions that predict the SBS-performance of that structure as well as the optimal operating conditions.

We acknowledge financial support from the Australian Research Council (ARC) via the Discovery Grant DP130100832, its Laureate Fellowship (Prof. Eggleton, FL120100029) program and the ARC Center of Excellence CUDOS (CE110001018).

A. Appendix: Expressions for inter-mode coupling

Within the main text, we restrict ourselves to intra-mode coupling with the goal of cleaner notation. In this appendix, we provide the corresponding results for the general case albeit at the expense of a great number of subscript indices. The governing equations (see Ref. [18]) for the general case of inter-mode coupling are:

$$\begin{aligned}
 s\partial_z P^{(1)} &= \underbrace{(\Gamma - 2\beta_{12} - \gamma_{122}P^{(2)})P^{(2)}P^{(1)} - \alpha_1 P^{(1)}}_{\text{small signal terms}} - \underbrace{(\beta_{11} + \gamma_{112}P^{(1)} + 4\gamma_{111}P^{(2)})[P^{(1)}]^2}_{\text{large signal corrections}}, \quad (16) \\
 \partial_z P^{(2)} &= \underbrace{-(\beta_{22} + \gamma_{222}P^{(2)})[P^{(2)}]^2 - \alpha_2 P^{(2)}}_{\text{small signal terms}} - \underbrace{(2\beta_{21} + \Gamma + 4\gamma_{221}P^{(2)} + \gamma_{211}P^{(1)})P^{(1)}P^{(2)}}_{\text{large signal corrections}}. \quad (17)
 \end{aligned}$$

Note that in contrast to intra-mode coupling, where the same loss coefficient (α , β , γ) appears in several terms, these symmetries are now lifted because the coefficient in each loss term is associated with a different combination of eigenmodes. These are the power-related coefficients required in Eqs. (16,17) and have been derived from the amplitude-related coefficients derived

in the Appendix of Ref. [18]:

$$\alpha_i = \frac{2\epsilon_0\omega}{\mathcal{P}^{(i)}} \int d^2r |\tilde{\mathbf{e}}^{(i)}|^2 \Im\{\epsilon_r\} , \quad (18)$$

$$\beta_{ij} = \frac{2}{\mathcal{P}^{(i)}\mathcal{P}^{(j)}} \int d^2r (|\tilde{\mathbf{e}}^{(i)} \cdot \tilde{\mathbf{e}}^{(j)}|^2 + |\tilde{\mathbf{e}}^{(i)} \cdot (\tilde{\mathbf{e}}^{(j)})^*|^2 + |\tilde{\mathbf{e}}^{(i)}|^2 |\tilde{\mathbf{e}}^{(j)}|^2) \Sigma^{2\text{PA}} , \quad (19)$$

$$\gamma_{ijk} = \frac{2}{\mathcal{P}^{(i)}\mathcal{P}^{(j)}\mathcal{P}^{(k)}} \int d^2r |\tilde{\mathbf{e}}^{(i)}|^2 \left[|\tilde{\mathbf{e}}^{(j)} \cdot \tilde{\mathbf{e}}^{(k)}|^2 + |\tilde{\mathbf{e}}^{(j)} \cdot (\tilde{\mathbf{e}}^{(k)})^*|^2 + |\tilde{\mathbf{e}}^{(j)}|^2 |\tilde{\mathbf{e}}^{(k)}|^2 \right] \Sigma^{\text{FCA}} . \quad (20)$$

Here, $\mathbf{e}^{(1/2)}$ represents the eigenmode patterns, $\mathcal{P}^{(1/2)}$ the corresponding power flux of the normalised eigenmode and $\Sigma^{2\text{PA}}$ and Σ^{FCA} are the nonlinear conductivities used to describe two-photon absorption (2PA) and 2PA-induced free carrier absorption (see Ref. [18]).

The Stokes power limit follows from the full Eq. (16) exactly in the same way as described in the main text:

$$P^{(1)} < \frac{\Gamma - 2\beta_{12}}{4\gamma_{12}} . \quad (21)$$

The figure of merit follows from the small signal terms of Eq. (16) alone, again exactly as described in the main text for the case of intra-mode coupling [note that the γ -coefficient appearing in the denominator is not necessarily the same as the one in Eq. (21)]:

$$\mathcal{F} = \frac{\Gamma - 2\beta_{12}}{2\sqrt{\alpha_1}\gamma_{122}} . \quad (22)$$